Applied Energy 334 (2023) 120740

Contents lists available at ScienceDirect

Applied Energy

journal homepage: www.elsevier.com/locate/apenergy

Coalitional model predictive control of parabolic-trough solar collector fields with population-dynamics assistance ☆

Ana Sánchez-Amores [a,*], Juan Martinez-Piazuelo [b], José M. Maestre [a], Carlos Ocampo-Martinez [b], Eduardo F. Camacho [a], Nicanor Quijano [c]

[a] Department of Systems and Automation Engineering, University of Seville, Spain
[b] Automatic Control Department, Universitat Politècnica de Catalunya, Spain
[c] Departamento de Ingeniería Eléctrica y Electrónica, Universidad de los Andes, Colombia

ARTICLE INFO

Keywords:
Model predictive control
Coalitional control
Population dynamics
Distributed solar collector field

ABSTRACT

Parabolic-trough solar collector fields are large-scale systems, so the application of centralized optimization-based control methods to these systems is often not suitable for real-time control. As such, this paper formulates a novel coalitional control approach as an appropriate alternative to the centralized scheme. The key idea is to split the overall solar collector field into smaller subsystems, each of them governed by a local controller. Then, controllers are clustered into coalitions to solve a local optimization-based problem related to the corresponding subset of subsystems, so that an approximate solution of the original centralized problem can be obtained in a decentralized fashion. However, the operational constraints of the solar collector field couple the optimization problems of the multiple coalitions, thus limiting the ability to solve them in a fully decentralized manner. To overcome this issue, a novel population-dynamics-assisted resource allocation strategy is proposed as a mechanism to decouple the local optimization problems of the multiple coalitions. The proposed coalitional methodology allows to solve the multiple local subproblems in parallel, hence reducing the overall computational burden, while guaranteeing the satisfaction of the operational constraints and without significantly compromising the overall performance. The effectiveness of proposed approach is shown through numerical simulations of a 10- and 100-loop version of the ACUREX solar collector field of *Plataforma Solar de Almería*, Spain.

1. Introduction

In 2015, all United Nations members approved the *2030 Agenda for Sustainable Development*, where seventeen sustainable development goals can be found. In particular, Goals #7 and #13, (“Affordable and clean energy” and “Climate action” respectively), focus on the need to tackle climate change and protect the environment [1], since carbon dioxide and other greenhouse gases in the atmosphere have reached record levels in recent years. For this reason, there is great interest in the use of renewable energy to reduce the high environmental impact of fossil fuel systems. Among the different sources of renewable energy (for example, solar, wind, geothermal, hydropower, ocean, bioenergy), solar energy is the most abundant [2]. To generate electricity from sunlight, two main techniques can be distinguished: directly through photovoltaic panels or indirectly using concentrated solar power (CSP) systems. CSP systems, reviewed in [3,4], collect solar radiation and concentrate it to heat a fluid that will produce steam to drive turbine generators. This technology includes parabolic troughs [5], Fresnel collectors [6], solar power towers [7], and dish collectors [8]. However, this article will focus exclusively on the control for parabolic-trough solar collector fields.

Unlike other power generation processes, where the main energy source can be handled as a control variable, solar energy cannot be manipulated and therefore acts as a disturbance from a control view point. In this regard, model predictive control (MPC) is one of the most

☆ The authors gratefully acknowledge the financial support by the European Research Council (ERC) under the European Union’s Horizon 2020 research and innovation program (OCONTSOLAR, grant agreement No 789051). In addition, the authors would like to thank the projects PID2020-119476RB-I00 (C3PO-R2D2), PID2020-115905RB-C21 (L-BEST), and TED2021-129927B-I00 (MASHED), funded by MCIN/ AEI/10.13039/501100011033 and by the European Union Next GenerationEU/PRTR, for supporting this research. Finally, Juan Martinez-Piazuelo gratefully acknowledges the Universitat Politècnica de Catalunya and Banco Santander, Spain for the financial support of his predoctoral grant FPI-UPC.

* Corresponding author.
E-mail addresses: asamores@us.es (A. Sánchez-Amores), juan.pablo.martinez.piazuelo@upc.edu (J. Martinez-Piazuelo), pepemaestre@us.es (J.M. Maestre), carlos.ocampo@upc.edu (C. Ocampo-Martinez), efcamacho@us.es (E.F. Camacho), nquijano@uniandes.edu.co (N. Quijano).

https://doi.org/10.1016/j.apenergy.2023.120740
Received 3 August 2022; Received in revised form 28 December 2022; Accepted 18 January 2023
Available online 24 January 2023
0306-2619/© 2023 The Author(s). Published by Elsevier Ltd. This is an open access article under the CC BY-NC-ND license (http://creativecommons.org/licenses/by-nc-nd/4.0/).

popular techniques applied in the control of parabolic-trough plants, as it deals with system disturbances and constraints in a receding-horizon fashion. For example, the authors of [9] formulate a dual MPC approach for reference tracking and disturbance rejection, while the authors of [10] propose an MPC for the optimal scheduling of CSP systems. However, one of the main drawbacks of the MPC approach is the computational effort required to solve large-scale optimization problems in real time. To overcome this issue in parabolic-through plants, recent research has focused on decreasing the computational burden with respect to the implementation of a centralized MPC. For example, neural networks are applied to approximate the optimal flow value given by an MPC in [11], reducing the computational load. Moreover, the authors of [12] propose a fuzzy MPC for the parabolic-trough plant to predict the future evolution of the outlet temperature while reducing the computational time with respect to the original non-linear model of the plant.

As an alternative, coalitional MPC partitions the large-scale system into clusters of local controllers (or agents), achieving a trade-off between coordination and performance. This type of distributed control dynamically adjusts the structure of the global problem, creating clusters of cooperative agents only when it improves overall performance. The main objective of coalitional control is to offer an intermediate solution between fully cooperative and decentralized schemes, providing better performance than decentralized control while reducing the communication and computation burden of fully cooperative approaches [13]. A major problem that arises in the application of centralized strategies to large-scale systems is that the number of control variables explodes while increasing the size of the model. To address this issue, coalitional control splits the global control problem into multiple local subproblems, which are solved in a decentralized fashion by the agents within a coalition. In particular, the local subproblems in a parabolic-trough solar collector field are coupled to each other by a global shared resource constraint, referring to the total amount of heat transfer fluid that can be provided to the field; see [14,15]. Hence, a key problem is how to decouple the shared constraint, so that the local problem of each coalition can be solved in a decentralized fashion and independently of other coalitions. In this way, such a decentralized framework seeks to reduce the computational burden of the overall approach by taking advantage of parallel executions. Note that, for classical decentralized schemes, the satisfaction of the coupled constraint requires an equal distribution of this constraint among all the local problems, without any dynamic adjustment, since there is no cooperation between the different parts of the system. As a result, there could be a greater loss of performance.

In contrast to previous works and inspired by ideas on evolutionary game theory, this paper proposes a novel approach to decouple the aforementioned shared resource constraint. Recently, the field of evolutionary games and population dynamics [16,17] has received significant attention with respect to applications of dynamic resource allocation in large-scale systems [18]. Some examples include wireless networks [19], water distribution systems [20], demand response applications [21], coordination of electric vehicle charging [22], and congestion games in autonomous vehicle fleets [23], among others. A motivation behind such applications is that population dynamics have certain invariance and stability features that make them suitable for dynamic resource allocation problems. Namely, granted an appropriate initial condition, some population dynamics guarantee the dynamic satisfaction of simplex-like constraints without relying on repeated projections. In the context of dynamic resource allocation, this invariance property can be exploited to guarantee the feasibility of the resource distribution at any point in time. On the other hand, several population dynamics have well-studied asymptotic stability properties, which guarantee their asymptotic convergence to the optimal solution of an underlying optimization problem [17].

Based on the above, this work combines a coalitional model predictive control approach with population dynamics for resource distribution. In particular, the coalitional approach splits the global control problem into multiple coupled local subproblems, whereas population dynamics are employed to allocate the available resource over the multiple coalitions, guaranteeing the satisfaction of the coupled constraint at any point in time so that the multiple local control subproblems can be solved in parallel to reduce computational time. In summary, the contributions of this paper are twofold:

- First, a novel coalitional MPC approach with population-dynamics assistance is formulated for the temperature regulation of parabolic-trough solar collector fields. The proposed approach not only guarantees the exact satisfaction of the shared resource constraint, but also reduces computational burden, leading to improved scalability for large-scale scenarios.
- Second, the proposed approach is validated through numerical simulations of a 10- and 100-loop version of the ACUREX solar collector field of the *Plataforma Solar de Almería*, Spain. The numerical results show that, when compared to a centralized MPC approach, the proposed method provides a significant reduction in computation times, yet with negligible losses on performance.

The proposed strategy is presented as an alternative to relieve the computational burden, since, apart from considering a coalition approach, it proposes a linearization of the lumped parameter model of the solar plant. In this way, the use of a nonlinear distributed parameter models is avoided as it would increase the overall computational burden. Another alternative on how to deal with the non-linearity of the system model can be found in [24], where the authors use a linear parameter varying model of the solar plant. In such a work, the authors present an adaptive MPC in which two consecutive quadratic programming problems are solved to obtain the optimal control law. In contrast with such an approach, our proposed strategy relies on static linearization techniques, reducing the overall computational burden of the method. On the other hand, it is worth to highlight that although our approach employs an additional control layer for the dynamic resource allocation of the coupled constraint (which may be seen as a disadvantage as it increases the overall complexity of the strategy), such a control layer can be executed at a different time-scale than the (bottom) MPC layer, ruling out any significant bottlenecks at real-time execution. Moreover, despite this additional complexity, our proposed approach reduces the total computation time in comparison with centralized MPC, with a minimal impact on the overall performance.

The remainder of this article is organized as follows. In Section 2, the mathematical model of the parabolic-trough solar collector field and the operational constraints considered are presented. Section 3 describes the overall control objective and introduces the problem setting for coalitional MPC. Furthermore, Section 3 motivates the assistance via population-dynamics to distribute the available resource and handle the coupled constraint, and presents the proposed control scheme. Section 4 includes some numerical simulation results on a 10- and 100-loop solar collector field. Finally, concluding remarks and future research lines are provided in Section 5.

Notations. $\mathbb{R}^n$ denotes the n-dimensional Euclidean space, while $\mathbb{R}^n_{\geq 0}$ and $\mathbb{R}^n_{>0}$ denote the non-negative and positive orthants of $\mathbb{R}^n$, respectively. Moreover, let $\mathrm{col}\,(a, b, \dots, z)$ denote the stacked column vector obtained from the collection of column vectors $a, b, \dots, z$. Similarly, let $\mathrm{diag}\,(A_1, A_2, \dots, A_N)$ be the diagonal block matrix with the square matrices $A_1, A_2, \dots, A_N$ in its main diagonal. Given a vector $a \in \mathbb{R}^n$, the notation a_i refers to the ith element of a. Finally, given a square matrix $A \in \mathbb{R}^{n\times n}$, the notation $\lambda_{\max}(A)$ refers to the maximum eigenvalue of A.

2. Parabolic-trough solar collector field

2.1. Description of the ACUREX solar plant system

Throughout this article, the ACUREX parabolic-trough solar collector field located in *Plataforma Solar de Almería* (PSA), Spain, is

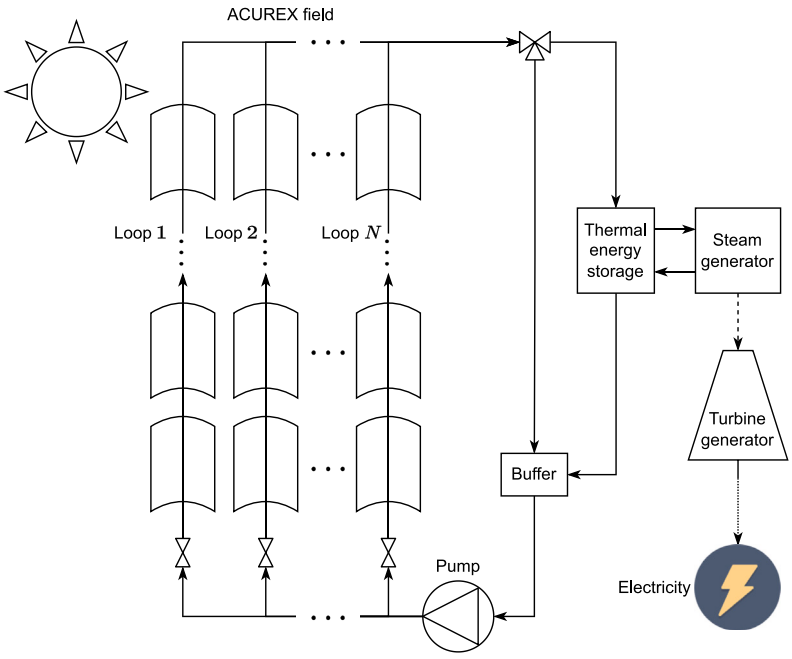

Fig. 1. Schematic of the ACUREX parabolic-trough solar collector plant.

studied. The solar field consists of a set of parabolic mirrors, known as collectors, which concentrate solar irradiance in a pipe located in its focal line, where a heat transfer fluid (HTF) heats up as it circulates. The HTF carries the thermal energy to produce steam, and the electrical energy is generated by a steam turbine. For this plant, Therminol 55 is used as the HTF, whose density (ρ) and specific heat capacity (c) are temperature dependent and are given by [25]

$$\begin{aligned} \rho\left(T_f(t)\right) &= 903 - 0.672T_f(t), \\ c\left(T_f(t)\right) &= 1820 + 3.478T_f(t), \end{aligned} \tag{1}$$

where $T_f(t)$ is the temperature of the HTF at time instant t.

The distributed collector field can be modeled as a set $\mathcal{L} = \{1, \dots, N\}$ of N parallel loops; in particular, the ACUREX solar collector field consists of 480 east–west aligned single-axis tracking collectors that form $N = 10$ loops. Each loop measures 174 m in length, and consists of four 12-module collectors connected in series. For each loop $j \in \mathcal{L}$, it is possible to distinguish an active part that receives solar irradiance (144 m length) from a passive part where solar radiation does not reach (30 m length). Moreover, it is assumed that the HTF inflow of each loop $j \in \mathcal{L}$ is controllable. Furthermore, in general, loops have different dynamics, because their mirrors might have different levels of cleanliness and thermal losses. However, there are some homogeneous parameters for all loops $j \in \mathcal{L}$, such as the length L of each loop, the cross-sectional area a_f of the HTF, and the reflective surface S of each loop. As an illustration, Fig. 1 shows a diagram of the ACUREX plant.

2.2. Concentrated parameter model

This section presents the dynamical model considered, which describes the behavior of the ACUREX solar plant [26]. For the sake of clarity, the model variables and parameters are summarized in Table 1.

In what follows, each loop $j \in \mathcal{L}$ will be described using the concentrated parameter model, which provides a global description of a loop by modeling the variation of the internal energy of the HTF. More formally, each loop $j \in \mathcal{L}$ can be described by the continuous-time model given by

$$\begin{aligned} C_j(t)\frac{dT_j(t)}{dt} =& \alpha_j \eta S I(t) - \beta_j S H_j(t)\left(\bar{T}_j(t) - T^a(t)\right) \\ & - P_j(t) q_j(t)\left(T_j(t) - T_j^{in}(t)\right), \end{aligned} \tag{2}$$

with

$$\begin{aligned} C_j(t) &= \rho_j\left(T(t)\right) c_j\left(T(t)\right) a_f L, \\ P_j(t) &= \rho_j\left(T(t)\right) c_j\left(T(t)\right), \\ \bar{T}_j(t) &= \frac{T_j(t) + T_j^{in}(t)}{2}. \end{aligned}$$

Here, the global coefficient of thermal losses $H_j(t)$ depends on the outlet (T_j), inlet (T_j^{in}), and ambient (T^a) temperatures, and its expression can be found in [25]. Moreover, η is the overall efficiency of the collectors, considering the optical and geometric efficiencies. In addition, the difference in loop dynamics is modeled through two scaling factors α_j and β_j that characterize the mirror cleanliness and thermal losses of each loop, respectively. Furthermore, notice that, as (2) describes the dynamics of the outlet temperature of loop j, the properties in (1) of the HTF in loop j become dependent on the corresponding outlet temperature $T_j(t)$.

2.3. Characteristics and operational constraints of the system

Let us assume that the inlet temperature of each loop is equal to the inlet temperature of the fluid to the field, i.e., $T_j^{in} = T^{in}$, for all $j \in \mathcal{L}$. Additionally, the inlet temperature, direct normal irradiance (DNI), and ambient temperature are considered disturbances that can be measured or estimated. Moreover, the outlet temperature of the whole field is given by

$$T(t) = \frac{\sum_{j=1}^{N} T_j(t) q_j(t)}{q^T(t)}, \tag{3}$$

where the total HTF flow of the field is defined as

$$q^T(t) = \sum_{j=1}^{N} q_j(t). \tag{4}$$

On the other hand, several operating restrictions must be considered due to the minimum ($T^{\min}$) and maximum ($T^{\max}$) temperatures supported by the HTF, and also the operating limits of the pump and valves. Namely, it is required that

$$T^{\min} \le T_j(t) \le T^{\max}, \quad \forall j \in \mathcal{L} \tag{5a}$$

$$q^{\min} \le q_j(t) \le q^{\max}, \quad \forall j \in \mathcal{L} \tag{5b}$$

Table 1
Model's variables (top) and parameters (bottom).

Symbol	Description	Units
t	Continuous-time variable	s
k	Discrete-time index	–
T_j	Outlet temperature of loop j	°C
T_j^{in}	Inlet temperature of loop j	°C
T	Outlet temperature of the field	°C
T^{in}	Inlet temperature of the field	°C
T^a	Ambient temperature	°C
$\bar{T}$	Mean inlet–outlet temperature	°C
q_j	HTF flow in loop j	l/s
q^T	Total HTF flow	l/s
I	Direct solar irradiance	W/m^2
H_j	Coef. of thermal losses of loop j	W/(m^2 °C)
δ	Discretization time	s
N	Number of loops	–
L	Length of each loop	m
S	Reflective surface of each loop	m^2
a_f	Cross-sectional area of the fluid	m^2
ρ	Density of the HTF	kg/m^3
c	Specific heat capacity of the HTF	J/(kg °C)
C_j	Thermal capacity of a loop	J/°C
η	Efficiency of the collectors	–
α_j	Cleanliness scale factor of loop j	–
β_j	Loss scale factor of loop j	–

$$q^T(t) \le q^{T,\max}, \tag{5c}$$

where the minimum flow value in a loop, $q^{\min}$, is such that there is a turbulent regime within the loop, and the maximum flow in a loop, $q^{\max}$, is related to the maximum pressure drop allowed. Moreover, the pump limits the total HTF flow of the field within a maximum value $q^{T,\max}$.

2.4. Linear discrete-time model of the system

For the control strategy formulated in this paper, a linearization of the concentrated parameter model of each loop, i.e., (2), is proposed to operate every loop close to a desired operating point $\left(T_j^\circ, q_j^\circ\right)$. For this purpose, the temperature and flow of each loop $j \in \mathcal{L}$ are redefined as the sum of its value at the operating point plus a small increment represented by the deviation variables (x_j, u_j). That is,

$$T_j(t) = T_j^\circ + x_j(t), \quad q_j(t) = q_j^\circ + u_j(t). \tag{6}$$

Assumption 1. Since only small variations around the operating point are considered, it is assumed that temperature-dependent parameters, e.g. P_j, C_j and H_j, are fixed at a temperature value equal to T_j°. Consequently, these time-varying parameters are now assumed to be constant. For the sake of clarity, these parameters are identified with the superscript ° in the linear model to emphasize their dependence on the operating point.

Based on (6), the lumped model defined in (2) can be expressed as

$$\begin{aligned} C_j^\circ \frac{dx_j(t)}{dt} = &-\left(P_j^\circ q_j^\circ + \frac{\beta_j S H_j^\circ}{2}\right) x_j(t) \\ &- P_j^\circ \left(T_j^\circ - T^{in}(t)\right) u_j(t) \\ &+ \alpha_j \eta S I(t) - P_j^\circ q_j^\circ \left(T_j^\circ - T^{in}(t)\right) \\ &- \frac{\beta_j S H_j^\circ}{2}\left(T_j^\circ + T^{in}(t) - 2T^a(t)\right), \end{aligned} \tag{7}$$

for every loop $j \in \mathcal{L}$. Moreover, by grouping and identifying the terms that accompany x_j as A_j^c, those that accompany u_j as B_j^c, and the disturbances as w_j^c, the model in (7) can be rewritten as

$$C_j^\circ \dot{x}_j(t) = A_j^c x_j(t) + B_j^c u_j(t) + w_j^c(t), \quad \forall j \in \mathcal{L}, \tag{8}$$

where the superscript c emphasizes the continuous-time nature of the model.

The forward Euler method is used to approximate the time derivatives in order to express the model of each loop $j \in \mathcal{L}$ in discrete time, that is,

$$\frac{dx_j(t)}{dt} \approx \frac{x_j[k+1] - x_j[k]}{\delta}, \tag{9}$$

being δ the discretization time. Dividing by C_j°, and following (9), Eq. (7) can be expressed in discrete time as

$$x_j[k+1] = \underbrace{\left(\frac{\delta}{C_j^\circ} A_j^c + 1\right)}_{A_j} x_j[k] + \underbrace{\frac{\delta}{C_j^\circ} B_j^c}_{B_j} u_j[k] + \underbrace{\frac{\delta}{C_j^\circ} w_j^c}_{w_j}[k], \tag{10}$$

for all $j \in \mathcal{L}$. By the identified terms, the local discrete-time model of each loop $j \in \mathcal{L}$ is given by

$$x_j[k+1] = A_j x_j[k] + B_j u_j[k] + w_j[k]. \tag{11}$$

Equivalently, by defining

$$\begin{aligned} x[k] &= \operatorname{col}\left(x_1[k], x_2[k], \dots, x_N[k]\right) \in \mathbb{R}^N, \\ u[k] &= \operatorname{col}\left(u_1[k], u_2[k], \dots, u_N[k]\right) \in \mathbb{R}^N, \\ w[k] &= \operatorname{col}\left(w_1[k], w_2[k], \dots, w_N[k]\right) \in \mathbb{R}^N, \\ A &= \operatorname{diag}\left(A_1, A_2, \dots, A_N\right) \in \mathbb{R}^{N\times N}, \\ B &= \operatorname{diag}\left(B_1, B_2, \dots, B_N\right) \in \mathbb{R}^{N\times N}, \end{aligned}$$

the model of the whole field can be written more compactly based on (11) as

$$x[k+1] = Ax[k] + Bu[k] + w[k]. \tag{12}$$

Finally, the constraints in (5) can be rewritten in terms of the deviation variables $x_j[k] = T_j[k] - T_j^\circ$ and $u_j[k] = q_j[k] - q_j^\circ$ as

$$T^{\min} - T_j^\circ \le x_j[k] \le T^{\max} - T_j^\circ, \quad \forall j \in \mathcal{L} \tag{13a}$$

$$q^{\min} - q_j^\circ \le u_j[k] \le q^{\max} - q_j^\circ, \quad \forall j \in \mathcal{L} \tag{13b}$$

$$\sum_{j\in\mathcal{L}} u_j[k] \le q^{T,\max} - \sum_{j\in\mathcal{L}} q_j^\circ. \tag{13c}$$

Remark 1. We highlight that since the control strategy formulated in this paper relies on the discrete-time linear time-invariant (LTI) model presented in (12), our proposed method is also applicable for other nonlinear models of the solar plant (i.e., models different than (2), for each loop $j \in \mathcal{L}$) for which a discrete-time LTI model as (12) can be obtained.

3. Problem statement and proposed approach

3.1. Overall control objective

This section introduces the overall control objective considered in this paper. Throughout, the linear discrete-time model of each loop given in (11) is considered, or equivalently, the model of the entire solar field given in (12). Both models are defined in terms of the deviation variables $x_j[k] = T_j[k] - T_j^\circ$ and $u_j[k] = q_j[k] - q_j^\circ$. Thus, the goal is to regulate the deviation variables at the origin, so that the system is kept close to the desired operating point (T_j°, q_j°), for all $j \in \mathcal{L}$, while satisfying the operational constraints given in (13).

Definition 1 (*Control Objective*). Let $N_p \in \mathbb{Z}_{\ge 1}$ be the prediction horizon. The model predictive optimization-based control problem to be solved at time k is given by

$$\min_{\mathbf{u}[k]} \sum_{n=1}^{N_p} x[k+n]^\top Q x[k+n] + \sum_{n=0}^{N_p-1} u[k+n]^\top R u[k+n], \tag{14}$$

subject to the constraints in (12) and (13). The weighting matrices for state and input $Q, R \in \mathbb{R}^{N\times N}$ are symmetric positive definite, and the vector $\mathbf{u}[k]$ describes the sequence of inputs $u[\cdot]$ from instants $n = k$ to $k + N_\mathrm{p} - 1$, i.e.,

$$\mathbf{u}[k] = \mathrm{col}\left(u[k], u[k+1], \dots, u[k+N_\mathrm{p}-1]\right).$$

Remark 2. Regarding Definition 1, it is worth highlighting that the corresponding model predictive controller receives an estimate of the solar DNI profile over the prediction horizon, which can be forecast using several techniques, such as those proposed in [27,28]. Furthermore, Assumption 2 is imposed to guarantee the existence of a solution.

Assumption 2. The set of solutions to the problem in Definition 1 is not empty. Moreover, $Nq^{\min} \leq q^{T,\max} \leq Nq^{\max}$.

Although the problem in Definition 1 could be solved by standard centralized methods, if the size of the solar field is sufficiently large, the computational burden of the underlying optimization problem might render the application of such centralized methods unfeasible for real-time control. As such, a coalitional control approach is formulated. The key idea is to group subsets of loops into so-called coalitions, and define a local (decoupled) optimization problem for each coalition, so that by solving these multiple (smaller) decoupled problems in parallel one obtains an approximate solution of the centralized problem in Definition 1. Consequently, through a trade-off between computational burden and performance, the centralized controller is replaced by a set of local controllers whose corresponding optimization problems have lower computational costs and can be solved in parallel in a decentralized fashion. The proposed coalitional method is detailed below.

3.2. Coalitional control approach

In what follows, we proceed as in previous coalitional control schemes in the solar plant framework [14,15].

Following graph-theoretic partitioning approaches [29], the parabolic-trough plant can be characterized by a graph $\mathcal{G} = (\mathcal{L}, \mathcal{E})$ that models a cooperative network. Being $\mathcal{L}$ the set of loops, it is assumed that a local controller or agent governs each loop $j \in \mathcal{L}$. Furthermore, $\mathcal{E}$ represents a set of links $\mathcal{E} \subseteq \mathcal{L} \times \mathcal{L}$ that establish data-exchange connections between the different loops. The state of these links is dynamically switched between enabled and disabled according to the needs of the system. When a given link is enabled, the corresponding loops are connected through a bidirectional flow of information, allowing their controllers to exchange data.

Assumption 3. At any time, the graph $\mathcal{G}$ is partitioned by a set of M disjoint complete subgraphs $\mathcal{G}_1, \mathcal{G}_2, \dots, \mathcal{G}_M$. More formally, for every $i \in \{1, 2, \dots, M\}$ it exists a subgraph $\mathcal{G}_i = (\mathcal{L}_i, \mathcal{E}_i)$, with $\mathcal{L}_i \subseteq \mathcal{L}$ and $\mathcal{E}_i = \mathcal{L}_i \times \mathcal{L}_i$. Also, $\mathcal{L}_i \cap \mathcal{L}_\ell = \emptyset$ holds for all $i \neq \ell$, and $\mathcal{L}_1 \cup \mathcal{L}_2 \cup \cdots \cup \mathcal{L}_M = \mathcal{L}$.

Definition 2 (*Coalition*)**.** Under the partitioning provided by Assumption 3, a coalition $C_i = \mathcal{L}_i$ is a subset of loops whose controllers are connected through a set of enabled links $\mathcal{E}_i$ according to the complete subgraph $\mathcal{G}_i$. In this regard, agents within a coalition operate as a single entity. In general, the size of a coalition can range from a singleton $C_i = j$, i.e., $|C_i| = 1$, to the grand coalition $C_i = \mathcal{L}$, i.e., $|C_i| = N$, where $|C_i|$ denotes the cardinality of C_i. Throughout, let $\mathcal{P} = \{C_1, C_2, \dots, C_M\}$ be the set of coalitions, and thus $\mathcal{P}$ characterizes the partition of the system.

Remark 3. The partitioning of the field can be done following different criteria such as geographical proximity, e.g., grouping loops that are close to each other in the solar plant; difference in the DNI, e.g., associating loops that receive more solar irradiance with those that are dirty or shaded; or simply by creating random coalitions. In particular, this article does not focus on a specific partitioning method. Instead, it is assumed that the partition $\mathcal{P}$ is given by an arbitrary previously selected criterion.

Based on the partition $\mathcal{P}$, the maximum HTF flow of the field (given in deviation variables by $q^{T,\max} - \sum_{j\in\mathcal{L}} q_j^\circ$) is distributed over the coalitions using a population-dynamics-assisted resource allocation method (the details of such a method are given in Section 3.3). Namely, let $q_{C_i}^{\max}$ denote the maximum HTF flow allowed for coalition $C_i \in \mathcal{P}$, and these maximum coalition-level flows are set to satisfy $\sum_{i=1}^{M} q_{C_i}^{\max} = q^{T,\max} - \sum_{j\in\mathcal{L}} q_j^\circ$. In terms of the deviation variables, it is thus required that

$$\sum_{j\in C_i} u_j[k] \leq q_{C_i}^{\max}, \quad \forall C_i \in \mathcal{P}. \tag{15}$$

Consequently, if the constraint in (15) holds in all coalitions, then the field-level constraint in (13c) is satisfied.

Therefore, assuming that an appropriate $q_{C_i}^{\max}$ has been determined for every coalition, the local control objective for each coalition is defined as follows.

Definition 3 (*Local Control Objective*)**.** The model predictive optimization-based control problem to be solved at time k by coalition $C_i \in \mathcal{P}$ is given by

$$\begin{aligned}\min_{\mathbf{u}_{C_i}[k]} \; & \sum_{n=1}^{N_\mathrm{p}} \sum_{j\in C_i} x_j[k+n] Q_j x_j[k+n] \\ & + \sum_{n=0}^{N_\mathrm{p}-1} \sum_{j\in C_i} u_j[k+n] R_j u_j[k+n],\end{aligned} \tag{16}$$

subject to (11), (13a), and (13b), for all $j \in C_i$, and (15). The local weighting scalars $Q_j, R_j \in \mathbb{R}_{\geq 0}$ are set according to the global weighting matrices in (14), for all $j \in C_i$. The vector $\mathbf{u}_{C_i}[k]$ describes the sequence of inputs within the coalition C_i from instants $n = k$ to $k + N_\mathrm{p} - 1$, i.e.,

$$\mathbf{u}_{C_i}[k] = \mathrm{col}\left(u_{C_i}[k], u_{C_i}[k+1], \dots, u_{C_i}[k+N_\mathrm{p}-1]\right),$$

where the vector $u_{C_i}[\cdot] = \mathrm{col}\left(\{u_j[\cdot]\}_{j\in C_i}\right)$ is comprised of the inputs of the loops belonging to coalition C_i.

Remark 4. By means of the maximum coalition-level flows $q_{C_i}^{\max}$, for all $C_i \in \mathcal{P}$, and the constraints in (15), the local control problems of Definition 3 are solved by each coalition in a decentralized fashion, i.e., independently of the other coalitions. Furthermore, Remark 2 also applies to each problem in Definition 3. On the other hand, it is worth highlighting that Assumption 2 is not enough to guarantee the non-emptiness of the set of solutions of each problem in Definition 3 under a general partition $\mathcal{P}$ and resource allocation $\left\{q_{C_i}^{\max}\right\}_{i=1}^{M}$. However, to overcome such an issue, the constraints in (13a) can be formulated as barrier functions whose corresponding weighting coefficients can be set locally by each coalition's controller (see, for instance, [14,15]).

Based on the discussion above, the question that remains to be answered is: how to determine $q_{C_i}^{\max}$, for all $C_i \in \mathcal{P}$, so that an appropriate approximation to the solution of the problem in Definition 1 can be obtained by means of solving the multiple decoupled problems in Definition 3? As such, to compute $q_{C_i}^{\max}$, for all $C_i \in \mathcal{P}$, we propose the population-dynamics-assisted resource allocation method presented below.

3.3. Population-dynamics-assisted resource allocation

This section formulates the proposed population-dynamics-assisted resource allocation method that is used to determine $q_{C_i}^{\max}$ for each

coalition $C_i \in \mathcal{P}$. In broad terms, the approach solves a model predictive optimization-based control problem with a unitary control horizon, whose solution provides an estimate of the average flow of HTF required by each loop over N_{p}, and thus provides information to determine $q_{C_i}^{\max}$, for all $C_i \in \mathcal{P}$, such that an approximate solution of the centralized problem in Definition 1 can be obtained by means of the coalitional control approach of Section 3.2. The solution of such a unitary control horizon problem is computed iteratively by exploiting certain properties of invariance and asymptotic stability of discrete-time population dynamics [30], and the numerical simulations in Section 4 show that the proposed method indeed leads to an acceptable trade-off between computational burden and performance. For the sake of clarity, we now proceed to describe in detail the proposed population-dynamics-assisted resource allocation method.

Throughout this section, the following model predictive control problem with unitary control horizon is considered.

Definition 4 (*Control Objective under Unitary Control Horizon*)**.** The unitary control horizon model predictive optimization-based control problem to be solved at time k is given by

$$v[k] = \arg\min_{u[k]} \sum_{n=1}^{N_{\mathrm{p}}} x[k+n]^{\top} Q x[k+n] + \sum_{n=0}^{N_{\mathrm{p}}-1} u[k]^{\top} R u[k], \tag{17}$$

subject to the constraints in (12), (13b), and the coupled constraint $\sum_{j\in\mathcal{L}} u_j[k] = q^{T,\max} - \sum_{j\in\mathcal{L}} q_j^{\circ}$. The weighting matrices for state and input, namely Q and R, are the same as those considered in Definition 1.

In contrast to the control problem of Definition 1, notice that the one in Definition 4 considers the constraint in (13c) with strict equality and disregards the constraints in (13a).[1] We enforce the constraint in (13c) with strict equality to allocate the totality of the available resource over the multiple coalitions, so that $\sum_{i=1}^{M} q_{C_i}^{\max} = q^{T,\max} - \sum_{j\in\mathcal{L}} q_j^{\circ}$. On the other hand, the reason to remove the constraints in (13a) is to guarantee the non-emptiness of the set of solutions under the unitary control horizon constraint. In particular, observe that under Assumption 2 it immediately follows that the set of solutions of the problem in Definition 4 is not empty. However, such a claim does not hold in general if the constraints in (13a) were to be considered in the problem of Definition 4. Clearly, one might deal with this issue by including the constraints in (13a) as penalty terms in (17), but such an approach increases the overall complexity of the method, as it involves the computation of additional penalty parameters, and increases the number of iterations required to guarantee the convergence of the proposed population dynamics to a solution (because a higher Lipschitz constant of (17) requires a smaller step size in the updates of the dynamics, c.f., [30, Theorem 5]). Finally, it is worth highlighting that Remark 2 also applies to the problem in Definition 4.

Now, note that according to the dynamics in (12), the state of the system at time instant $k+n$ under a constant input $u[k]$ applied during times $k, k+1, \dots, k+n-1$ is given by

$$x[k+n] = A^n x[k] + G_n u[k] + d[k+n-1], \quad \forall (k+n) \geq 1,$$

where

$$G_n = \sum_{\ell=0}^{n-1} A^{\ell} B$$

$$d[k+n-1] = \sum_{\ell=0}^{n-1} A^{\ell} w[k+n-1-\ell].$$

[1] Nevertheless, recall that the constraints in (13a) are still considered at the local level of each coalition's controller (see Remark 4).

Consequently, the cost function in (17) can be equivalently written as

$$\begin{aligned} J(u[k]) = \sum_{n=1}^{N_{\mathrm{p}}} \Big(& x[k]^{\top} A^{n\top} Q A^n x[k] + 2x[k]^{\top} A^{n\top} Q G_n u[k] \\ & + 2x[k]^{\top} A^{n\top} Q d[k+n-1] + u[k]^{\top} G_n^{\top} Q G_n u[k] \\ & + 2u[k]^{\top} G_n^{\top} Q d[k+n-1] \\ & + d[k+n-1]^{\top} Q d[k+n-1] \Big) + N_{\mathrm{p}} u[k]^{\top} R u[k], \end{aligned}$$

and the gradient of $J(\cdot)$ with respect to $u[k]$, which is denoted as $g(\cdot)$, is given by

$$\begin{aligned} g(u[k]) = \sum_{n=1}^{N_{\mathrm{p}}} \Big(& 2G_n^{\top} Q A^n x[k] + 2G_n^{\top} Q G_n u[k] \\ & + 2G_n^{\top} Q d[k+n-1] \Big) + 2N_{\mathrm{p}} R u[k]. \end{aligned}$$

Based on these formulations and motivated by the results in [30], to solve the problem in Definition 4 the following iterative dynamics (with state $\bar{v}[\kappa] = \mathrm{col}\left(\bar{v}_1[\kappa], \bar{v}_2[\kappa], \dots, \bar{v}_N[\kappa]\right)$ and output $v[\kappa] = \mathrm{col}\left(v_1[\kappa], v_2[\kappa], \dots, v_N[\kappa]\right)$) are considered

$$\vartheta_j[\kappa] = \max\left(q^{\max} - q^{\min} - \bar{v}_j[\kappa], 0\right) \tag{18a}$$

$$\varrho_{ij}[\kappa] = \min\left(\max\left(g_i(v[\kappa]) - g_j(v[\kappa]), 0\right), \gamma\right) \tag{18b}$$

$$\mu_j[\kappa] = \sum_{i\in\mathcal{L}} \left(\bar{v}_i[\kappa]\vartheta_j[\kappa]\varrho_{ij}[\kappa] - \bar{v}_j[\kappa]\vartheta_i[\kappa]\varrho_{ji}[\kappa]\right) \tag{18c}$$

$$\bar{v}_j[\kappa+1] = \bar{v}_j[\kappa] + \epsilon\mu_j[\kappa] \tag{18d}$$

$$v_j[\kappa] = \bar{v}_j[\kappa] + q^{\min} - q_j^{\circ}, \tag{18e}$$

for all $i, j \in \mathcal{L}$, where $\gamma, \epsilon \in \mathbb{R}_{>0}$ are strictly positive constants whose values are defined in Theorem 1, and the initial condition $\bar{v}[0]$ satisfies that

$$\bar{v}[0] \in \left\{ \bar{v} \in \mathbb{R}^N_{\geq 0} : \begin{array}{l} \sum_{j\in\mathcal{L}} \bar{v}_j = q^{T,\max} - N q^{\min} \\ \bar{v}_j \leq q^{\max} - q^{\min}, \quad \forall j \in \mathcal{L} \end{array} \right\}. \tag{19}$$

Moreover, it is worth to highlight that the updates in (18) occur at discrete-time instants κ, which are not necessarily the same time instants k of the discrete-time model in (12). Finally, given the partition $\mathcal{P}$, the resource allocation for each coalition $C_i \in \mathcal{P}$ at time κ is calculated as

$$q_{C_i}^{\max}[\kappa] = \sum_{j\in C_i} v_j[\kappa]. \tag{20}$$

The iterative dynamics in (18) correspond to a discretization of the so-called Smith population dynamics with carrying capacities [31], which are a particular case of the population dynamics studied in [30, 32], and whose evolutionary game theoretical interpretation is as follows.

Remark 5 (*Interpretation of the Dynamics in (18)*)**.** Population dynamics describe the temporal evolution of the strategic interaction of a large population of non-descriptive players under the mean-field approximation [17], i.e., assuming an infinite number of players modeled as continuum of a given mass. Under such a framework, $\bar{v}_j(t) \in \mathbb{R}_{\geq 0}$ represents the mass of players choosing strategy $j \in \mathcal{L}$ at the continuous-time $t \in \mathbb{R}_{\geq 0}$ (notice that the set of loops $\mathcal{L}$ is interpreted as the set of strategies of the game), and the temporal evolution of $\bar{v}_j(t)$ is given by the (mean) evolutionary dynamics model

$$\dot{\bar{v}}_j(t) = \sum_{i\in\mathcal{L}} \left(\bar{v}_i(t)\vartheta_j(t)\varrho_{ij}(t) - \bar{v}_j(t)\vartheta_i(t)\varrho_{ji}(t)\right).$$

Here, $\vartheta_j(t) \in \mathbb{R}_{\geq 0}$ denotes the carrying capacity of strategy j at time t (with $\vartheta_j(t) = 0$ meaning that no more players can choose strategy j at time t), and $\varrho_{ij}(t) \in \mathbb{R}_{\geq 0}$ is the switch rate of players from strategy i to strategy j at time t. Hence, $\bar{v}_i(t)\vartheta_j(t)\varrho_{ij}(t)$ is the mass of players switching from strategy i to strategy j at time t, while $\bar{v}_j(t)\vartheta_i(t)\varrho_{ji}(t)$ is the mass

of players switching from strategy j to strategy i at time t. Adding these terms over all strategies $i \in \mathcal{L}$ gives the total variation $\mu_j(t) \triangleq \dot{v}_j(t)$ of the mass of players playing strategy j at time t. Furthermore, to ease the practical application of the dynamics, the above continuous-time evolutionary dynamics model is discretized following a forward Euler discretization with step-size $\epsilon \in \mathbb{R}_{>0}$, as in (18d). In addition, to relate the population dynamics to the underlying optimization problem, the carrying capacity $\vartheta_j[\kappa]$ is set according to the HTF capacity of loop j, as in (18a); and the strategic switch rate $\varrho_{ij}[\kappa]$ is defined based on the gradients of the cost function $J(\cdot)$ and the saturation parameter $\gamma \in \mathbb{R}_{>0}$, as in (18b). Finally, employing (18e), the variable $\bar{v}_j[\kappa] \in [0, q^{\max} - q^{\min}]$ is shifted to $v_j[\kappa] \in [q^{\min} - q_j^{\circ}, q^{\max} - q_j^{\circ}]$, so that (13b) is satisfied. Overall, the dynamics in (18) comprise a population-dynamics-inspired iterative algorithm to update the variables $v_j[\kappa]$, for all $j \in \mathcal{L}$, which are in turn related to the solution of (17). For further details on how to apply population dynamics to solve convex optimization problems, as well as on the related analogies, we refer the interested reader to [18].

As mentioned above, our interest on the dynamics in (18) is to exploit certain invariance and asymptotic stability properties that these dynamics have. For the sake of completeness, such properties are formalized next.

Theorem 1. *Consider the iterative dynamics in (18) with*

$$\gamma = 2\left(q^{T,\max} - N q^{\min}\right)\lambda_{\max}\left(\sum_{n=1}^{N_p} G_n^{\top} Q G_n + N_p R\right),$$

and $0 < \epsilon < \left(\gamma\left(q^{\max} - q^{\min}\right)(N-1)\right)^{-1}$. *Moreover, let* $\bar{v}[0]$ *satisfy the condition in (19). The following facts hold.*

(1) For all $\kappa \geq 0$, *the vector* $v[\kappa]$ *satisfies the constraints of the problem in Definition 4.*

(2) The set of solutions of the problem in Definition 4 is asymptotically stable under the considered dynamics.

(3) For all $\kappa \geq 0$, *if* $v[\kappa]$ *is not a solution of the problem in Definition 4, then* $J(v[\kappa+1]) < J(v[\kappa])$.

Proof. Fact (1) follows immediately from [30, Theorem 3]. Namely, following the same steps as in the proof of [30, Theorem 3], one can show that under the given conditions for γ, ϵ, and $\bar{v}[0]$, the set in (19) is positively invariant under the discrete-time dynamics in (18d). That is, if $\bar{v}[0]$ satisfies (19), then $\bar{v}[\kappa]$ belongs to the set in (19), for all $\kappa \geq 0$. Consequently, by (18e) it holds that

$$q^{\min} - q_j^{\circ} \leq v_j[\kappa] \leq q^{\max} - q_j^{\circ}, \quad \forall j \in \mathcal{L}$$
$$\sum_{j\in\mathcal{L}} v_j[\kappa] = q^{T,\max} - \sum_{j\in\mathcal{L}} q_j^{\circ},$$

for all $\kappa \geq 0$, which means that the vector $v[\kappa]$ indeed satisfies the constraints of the problem in Definition 4, for all $\kappa \geq 0$.

Similarly, Facts (2) and (3) also follow from [30]. More precisely, following the formulation in Remark 5 and [30, Section 3], it holds that the discrete-time dynamics in (18a)–(18d) can be rewritten compactly as $\bar{v}[\kappa+1] = \bar{v}[\kappa] + \epsilon \mathbf{L}[\kappa]\mathbf{f}[\kappa]$, where $\mathbf{f}[\kappa] = -g(v[\kappa])$ and $\mathbf{L}[\kappa] \in \mathbb{R}^{N\times N}$ is a symmetric positive semi-definite matrix, for all $\kappa \geq 0$ [30, Lemma 1]. Also, based on (18e), the output vector $v[\kappa]$ is a constant shift of the state vector $\bar{v}[\kappa]$, for all $\kappa \geq 0$. Hence, consider the (convex quadratic) Lyapunov function candidate given by $V(v[\kappa]) = J(v[\kappa]) - J(v^*)$, where v^* is an arbitrary optimal solution of the problem in Definition 4. Following the same steps as in the proof of [30, Theorem 5] it can be shown that

$$V(v[\kappa+1]) - V(v[\kappa]) \leq -\epsilon(1-\epsilon\theta)\mathbf{f}[\kappa]^{\top}\mathbf{L}[\kappa]\mathbf{f}[\kappa],$$

where $\theta = \gamma\left(q^{\max} - q^{\min}\right)(N-1)$. Moreover, from [30, Lemma 1] and [30, Theorem 1], one can conclude that $\mathbf{f}[\kappa]^{\top}\mathbf{L}[\kappa]\mathbf{f}[\kappa] = 0$ if and only if $v[\kappa] = v^*$, and that $v[\kappa+1] = v[\kappa]$ if and only if $v[\kappa] = v^*$. Thus, if $0 < \epsilon < 1/\theta$, then $V(v[\kappa+1]) - V(v[\kappa]) < 0$, for every $v[\kappa+1] \neq v[\kappa] \neq v^*$. Consequently, v^* is asymptotically stable under the dynamics in (18) and Fact (2) holds. Also, Fact (3) holds from the previous Lyapunov stability analysis by noting that $V(v[\kappa+1]) - V(v[\kappa]) = J(v[\kappa+1]) - J(v[\kappa])$. ■

Based on Theorem 1, note that if the constraint in (19) is satisfied, then the feasible set of the problem in Definition 4 is positively invariant under the dynamics in (18), which in turn implies that the resource allocation in (20) always satisfies $\sum_{i=1}^{M} q_{C_i}^{\max} = q^{T,\max} - \sum_{j\in\mathcal{L}} q_j^{\circ}$, as desired. In addition, such a property holds without relying on recursive projections onto the feasible set, which simplifies the execution of the proposed dynamics. Furthermore, the cost function in (17) strictly decreases under the trajectories of the dynamics in (18), and its minimizer is achieved asymptotically. Thus, under the dynamics in (18), the resource allocation $v[\kappa_2]$ at time κ_2 is always better, in the sense of the problem in Definition 4, than the allocation $v[\kappa_1]$ at time κ_1, for all $0 \leq \kappa_1 < \kappa_2$ and granted that the allocation at time κ_1 is not optimal (in this case $v[\kappa_2] = v[\kappa_1]$). These facts show that, regardless of the number of update iterations applied to the dynamics in (18), the corresponding resource allocation is always better than the initial one (again, here better is to be understood in the sense of the problem in Definition 4). This property is attractive in the scenario where the updates in (18) can only be executed a limited number of times due to real-time constraints. Moreover, note that this property does not hold under other iterative approaches, such as the so-called primal–dual gradient dynamics [33], where the feasibility of the solution is guaranteed only in the asymptotic sense.

For clarity, a summary of the proposed general approach is provided below.

3.4. Summary of the proposed approach

The proposed coalitional model predictive control approach consists of two layers. At the top layer, the population-dynamics-assisted resource allocation method of Section 3.3 is employed to solve the unitary control horizon problem of Definition 4, and to allocate the resource $q_{C_i}^{\max}$ to each coalition $C_i \in \mathcal{P}$. At the bottom layer, on the other hand, the controller of each coalition $C_i \in \mathcal{P}$ solves the local model predictive control problem of Definition 3 subject to the resource allocation provided by the top layer. Both layers can be executed at different time-scales, so that the bottom layer uses the most up-to-date value of $q_{C_i}^{\max}$ when required. For completeness, the proposed approach is summarized in Algorithm 1.

Remark 6. The parameters N_{iter}, t_{top}, and t_{bot} in Algorithm 1 are set according to the computational capacities of the corresponding controllers, as well as to the associated time-scales of the solar plant. In particular, the time-scale t_{bot} is set as a multiple of the discretization time δ of the model, while the time-scale t_{top} is set as a multiple of t_{bot}. The rationale for setting t_{top} slower than t_{bot} is to avoid recomputing the resource allocation and partitioning of the system too frequently, and thus to reduce the computational burden of the overall approach. In fact, to further reduce the computational burden, the upper control layer might be executed in an event-triggered fashion based on the DNI disturbances.

4. Numerical simulations

This section provides simulation results on a 10 and 100 loop parabolic-trough solar plant such as the one described in Section 2. The control objective is to operate the plant around a desired operating temperature of 250 °C, while satisfying the coupled constraint in the total HTF flow, as well as the remaining operational constraints. All simulations have been performed using Matlab® R2020.a on a Windows 4.1 GHz hexa-core Intel® Core™ i7-8750H CPU and 16 GB RAM computer. Hereafter, the results obtained with the proposed coalitional

Algorithm 1 Overall control scheme.

The top and bottom control layers are repeatedly executed at possibly different time-scales.

Top control layer (executed at a time-scale t_{top})

1. Given an initial condition $\bar{v}[0]$ satisfying (19), the dynamics in (18) are updated a number of N_{iter} iterations. The resulting vector $v[N_{\text{iter}}]$ provides a feasible approximation for the solution of the problem in Definition 4 (with the error of the approximation converging to 0 as $N_{\text{iter}} \to \infty$).
2. The field partition $\mathcal{P}$ is computed by forming coalitions using the selected criterion (see Remark 3).
3. The resource allocation for each coalition $\mathcal{C}_i \in \mathcal{P}$ is computed by means of (20). Namely,

$$q_{\mathcal{C}_i}^{\max}[N_{\text{iter}}] = \sum_{j \in \mathcal{C}_i} v_j[N_{\text{iter}}], \quad \forall \mathcal{C}_i \in \mathcal{P}.$$

Bottom control layer (executed at a time-scale t_{bot})

1. For every coalition $\mathcal{C}_i \in \mathcal{P}$, the local optimization problem in Definition 3 is solved. Such a local optimization problem is subject to the (most up-to-date) resource allocation provided by the top layer, and its solution corresponds to the profile $\mathbf{u}_{\mathcal{C}_i}^*[k]$, where k denotes the current time instant under the time-scale t_{bot}.
2. Every coalition $\mathcal{C}_i \in \mathcal{P}$ applies the first component of the optimal sequence $\mathbf{u}_{\mathcal{C}_i}^*[k]$ to its associated loops (the deviation variables are transformed back to the original inputs by adding their corresponding operating values).

approach, summarized in Algorithm 1, are compared to those obtained with a centralized MPC. For this purpose, the index **P** is introduced to measure the performance of a given control algorithm throughout the entire simulation. The selected performance index is formulated as

$$\mathbf{P} = \sum_{k=0}^{T_{\text{sim}}} x[k+1]^\top Q x[k+1] + u[k]^\top R u[k], \tag{21}$$

where the simulation length is set to $T_{\text{sim}} = 60$min for both case studies. Moreover, a one-hour DNI profile[2] is used to model the disturbances, while the ambient temperature T^a and the inlet temperature T^{in} of the HTF to the field are considered constant for simplicity. As shown in the DNI profiles of Figs. 2 and 6, if the total length of a loop is discretized into one-meter segments, the passive parts of the loops correspond to the segments {37–42}, {79–96}, and {133–138}, respectively. Since these segments are not reached by concentrated solar radiation, their DNI is set to 0. Finally, Table 2 includes the values of the homogeneous parameters for all loops, and the values of operational constraints, which are taken equal for both simulations.

For these numerical simulations, the partition $\mathcal{P}$ of the field is calculated by grouping sets of $|\mathcal{C}_i|$ *unbalanced* loops according to the effective solar irradiance they receive. For instance, loops that are dirty or shaded due to a cloud are associated with loops that receive more DNI, either because they are not affected by any cloud or because they are cleaner. Moreover, let us assume that all coalitions have the same number of loops, i.e., $|\mathcal{C}_i| = |\mathcal{C}_\ell|$, for all $i, \ell \in \{1, 2, \dots, M\}$ with $i \neq \ell$.

On the other hand, to compare the coalitional and centralized control strategies by means of the required computational time, τ_{comp} is defined as the average computation time in the simulation, calculated as

$$\tau_{\text{comp}} = \frac{\sum_{k=1}^{T_{\text{sim}}} \tau[k]}{T_{\text{sim}}}, \quad \text{with} \quad \tau[k] = \frac{\sum_{\mathcal{C}_i \in \mathcal{P}} \tau_{\mathcal{C}_i}[k]}{|\mathcal{P}|}, \tag{22}$$

[2] The considered DNI profile is generated as in [34].

Table 2
Parameters (top) and constraints (bottom) of ACUREX field.

Symbol	Value	Units
L	174	m
S	267.4	m^2
a_f	$7.55 \cdot 10^{-4}$	m^2
η	0.64	–
α_j	[0.6, 1]	–
β_j	[1, 1.25]	–
$T^{\min}$	220	°C
$T^{\max}$	300	°C
$q^{\min}$	0.2	l/s
$q^{\max}$	1.5	l/s

Table 3
Time comparison for the centralized and coalitional simulations of the 10 and 100 loop plants.

Strategy	τ_{comp}	σ_{comp}	Units
Cen. MPC $N = 10$	0.2804	0.0466	s
Coal. MPC $N = 10$	0.1463	0.0154	s
Cen. MPC $N = 100$	2.7260	0.4522	s
Coal. MPC $N = 100$	0.2511	0.0045	s

where $\tau[k]$ is the average computation time per coalition at the time instant k, and $\tau_{\mathcal{C}_i}[k]$ is the time it takes for the coalition $\mathcal{C}_i$ to solve the local optimization problem in Definition 3. Seeking to be more rigorous with the results provided, Table 3 shows, in addition to the average computation time τ_{comp}, the value of the standard deviation σ_{comp} of the sample. The times included in Table 3 are measured in seconds.

4.1. Simulation results for the 10-loop field

The first case of study corresponds to the 10-loop ACUREX field located in the PSA. This scenario considers $q^{T,\max} = 5.7209$ l/s as the maximum flow value, which corresponds to the total HTF flow at the desired operating point of the system. Moreover, without loss of generality, five coalitions of two loops are considered. That is, $M = 5$ and $|\mathcal{C}_i| = 2$, for all $\mathcal{C}_i \in \mathcal{P}$.

For this simulation, two moving clouds have been generated for the DNI profile, which cross the field at specific times. As shown in Fig. 2, a small cloud moves through the plant between $t = 13$ min and $t = 26$ min, and a larger one appears between $t = 38$ min and $t = 52$ min. These clouds produce a decrease in the solar radiation received by the shaded loops, which in turn has an impact on the partition $\mathcal{P}$ of the field (as loops are grouped according to the effective DNI that they receive). As an illustration, the coalitional topology of the entire simulation is depicted in Fig. 3, where it can be seen that if the plant is not affected by the presence of any cloud, then the coalitions remain constant, but when a cloud enters the field, the partition $\mathcal{P}$ of the system changes, resulting in new coalitions. Finally, it is worth to highlight that besides the two moving clouds, it has been considered that some loops' collectors might be cleaner than others, and thus receive more solar radiation. This fact adds more heterogeneity to the components of the field.

In Fig. 4, the top plot shows the evolution over time of the outlet temperature of each loop, while the bottom plot depicts the evolution of the HTF flow circulating through each loop. Here, loops that have cleaner collectors and are therefore more efficient, have a higher flow value at the operating point q_j° (see, for example, that flows in loops #1 or #6 converge to a value q_j far above the corresponding values in loops #3 or #5). In addition, the passing of the larger cloud has a greater impact on both the temperature and the flows of the system, when compared to the passing of the smaller cloud (as expected). Moreover, such an impact is more notable in the less efficient loops (see, for

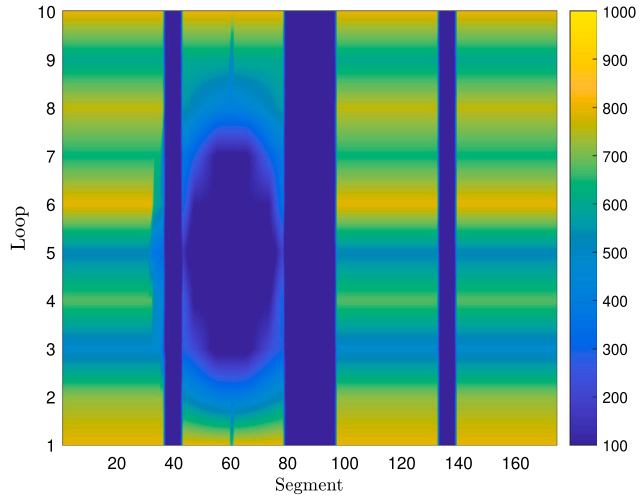

(a) Cloud passing at $t = 20$min

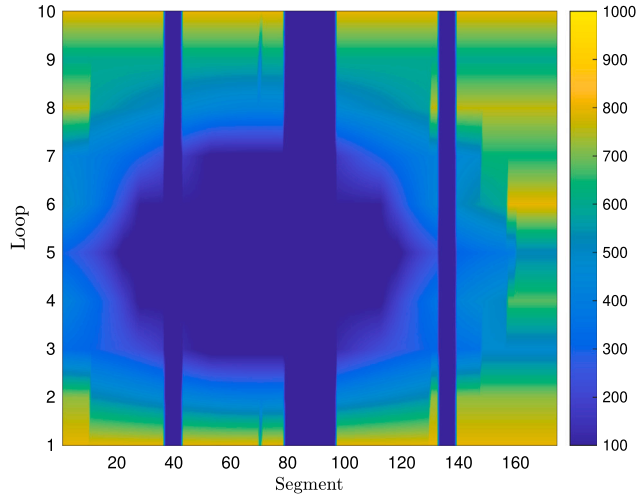

(b) Cloud passing at $t = 45$min

Fig. 2. Effective DNI profile of the 10-loop collector field with clouds passing.

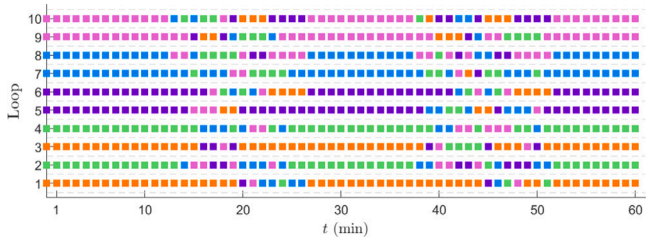

Fig. 3. Coalition forming of the 10-loop collector field.

example, the drop in the outlet temperature of loop #3, represented by a pink line in Fig. 4, when the second cloud appears).

A comparison of the proposed coalitional approach with respect to the centralized approach is presented in Fig. 5 in terms of the outlet temperature and the total HTF flow of the field. We highlight that the temporal evolution of both $T(t)$ and $q^T(t)$ under the coalitional approach follows up closely the ones of the centralized solution. In fact, the proposed coalitional algorithm results only in a 1.1771% drop in the overall performance $\mathbf{P}$ with respect to the centralized solution.

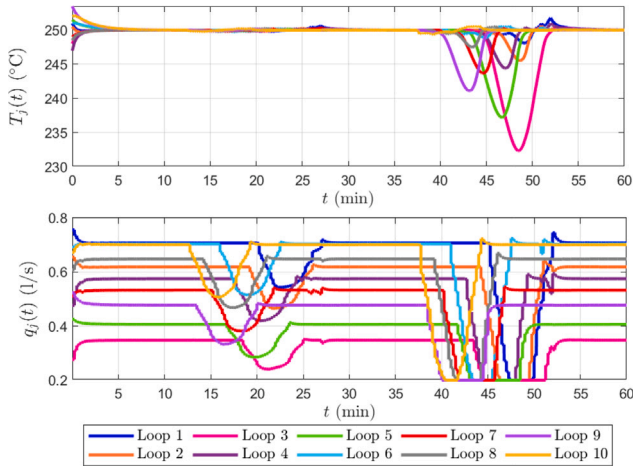

Fig. 4. Outlet temperature (top plot) and HTF flow (bottom plot) for each loop $j \in \{1, 2, \ldots, 10\}$ in the 10-loop field, when using the coalitional approach.

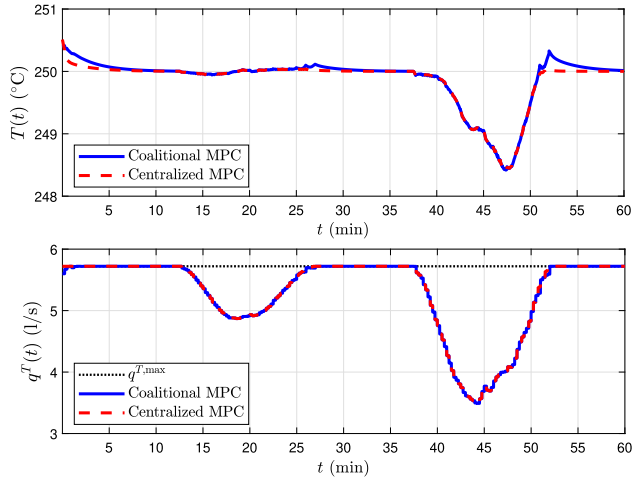

Fig. 5. Outlet temperature (top plot) and total HTF flow (bottom plot) of the 10-loop field. Solid lines represent the evolution using the proposed coalitional algorithm, while dashed lines represent the result using a centralized MPC. Here, the coupled constraint $q^{T,\max}$ is represented with a dotted line, and $T(t)$ and $q^T(t)$ are given by (3) and (4), respectively.

Likewise, as shown in Table 3, the computational time of the coalitional approach is lower than that of the centralized strategy, reducing the centralized time by half. This result is expected because the centralized approach solves the problem in Definition 1 using a single controller, whereas the coalitional one employs $N/|\mathcal{C}_i|$ decentralized controllers to solve the local problems of Definition 3 in parallel.

4.2. Simulation results for the 100-loop field

Let us now consider a 100-loop extension of the original 10-loop ACUREX field. As such, the values of the local constraints in (5) are also set according to Table 2, yet, since the number of loops is ten times greater, the value of $q^{T,\max}$ is set an order of magnitude higher than the 10-loop plant. Likewise, the maximum flow value in the plant is considered equal to $q^{T,\max} = 53.8834$ l/s, which corresponds to the total HTF flow at the desired operating point of the system. Besides, without loss of generality, in this scenario ten coalitions of ten loops are considered. That is, $M = 10$ and $|\mathcal{C}_i| = 10$, for all $\mathcal{C}_i \in \mathcal{P}$.

For this simulation, the DNI profile generates two moving clouds that cross over the 100-loop field. A large cloud moves through the plant almost during the whole simulation, between $t = 4$ min and

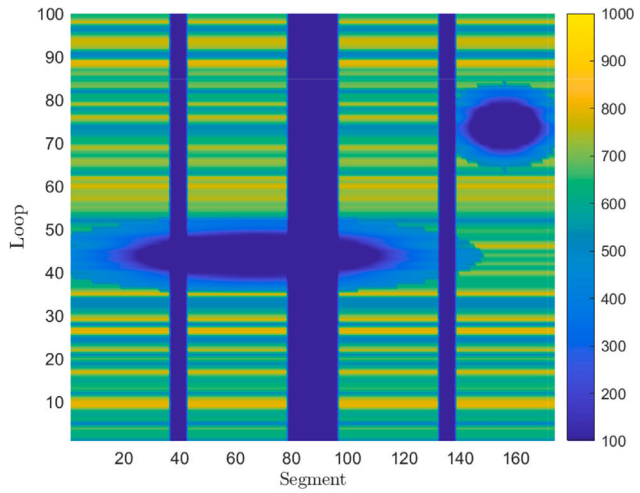

Fig. 6. Effective DNI profile of the 100-loop collector field with clouds passing at $t = 30$ min.

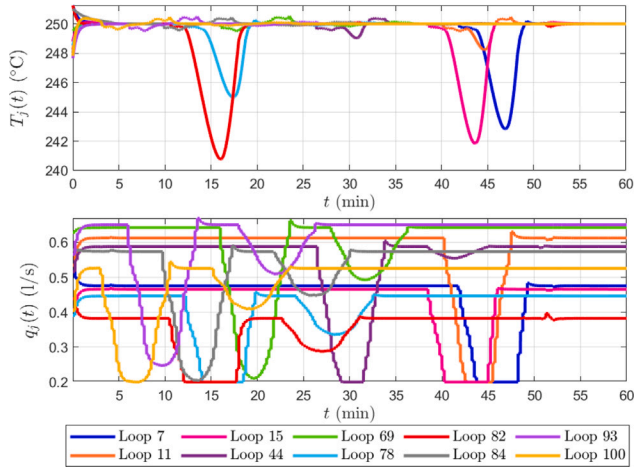

Fig. 7. Outlet temperature (top plot) and HTF flow (bottom plot) for 10 random loops in the 100-loop field, when using the coalitional approach.

$t = 52$ min, while a smaller cloud appears between $t = 16$ min and $t = 46$ min. As an illustration, Fig. 6 shows the two clouds over the plant halfway through the simulation, at $t = 30$ min. In addition, as before, it is considered that some loop collectors may be cleaner than others and therefore receive more solar radiation.

Fig. 7 shows the evolution over time of the outlet temperature $T_j(t)$ and the HTF flow $q_j(t)$ of ten random loops of the 100-loop plant. The small cloud crosses diagonally, affecting approximately the upper half of the field, while the large cloud crosses the entire plant, creating shadows on all of the loops. The consequences of passing clouds can be seen in Fig. 7. As in the case of the 10-loop plant, the most efficient loops stabilize in a higher flow value. See, for example, in the upper part of the field, loop #93 (light-purple line) reaches a higher value of the flow than loop #82 (red line). Similarly, when clouds shade loop #82, the drop in the outlet temperature of this loop is much greater than when #93 is affected by the clouds. The effects of cloud passing can also be seen in the evolution of the flow, as loops tend to decrease their flow $q_j(t)$ when they are shaded.

Finally, Fig. 8 compares the evolution of the outlet temperature and the total HTF flow of the 100-loop field when applying a centralized controller (dashed lines) and the proposed coalitional approach (solid lines). Note that, as the larger cloud crosses the field during almost the

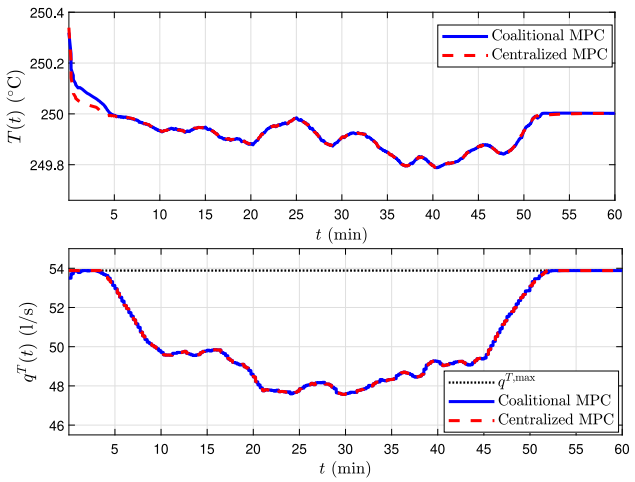

Fig. 8. Outlet temperature (top plot) and total HTF flow (bottom plot) of the 100-loop field. Solid lines represent the evolution using the proposed coalitional algorithm, while dashed lines represent the result using a centralized MPC. Here, the coupled constraint $q^{T,\max}$ is represented with a dotted line, and $T(t)$ and $q^T(t)$ are given by (3) and (4), respectively.

entire simulation, the outlet temperature is slightly below the desired value of 250 °C, while the total flow of the field suffers a notorious decrease with respect to the value of $q^{T,\max}$. However, the coalitional algorithm manages to closely follow the centralized evolution of $T(t)$ and $q^T(t)$ with a practically negligible loss in overall performance **P** of a 0.3544%.

Working with a larger plant involves longer computation times when optimizing the centralized MPC, as Table 3 shows. In this way, the coalitional control approach achieves better overall computation times, as it distributes the global problem among the set of local controllers given by the partition $\mathcal{P}$. Hence, the benefits of applying a coalitional control scheme are more notable as the system becomes larger in scale. In particular, choosing a smaller number of loops within a coalition $|C_i| < 10$ results in a lower average computation time τ_{comp}, but requires more local controllers to work simultaneously. For comparison, the 100-loop plant has been simulated with coalitions of 5 loops, $|C_i| = 5$, resulting in a decrease in **P** of a 0.4875%, with $\tau_{\text{comp}} = 0.1928$s and $\sigma_{\text{comp}} = 0.0176$s.

5. Concluding remarks

The proposed coalitional approach allows us to distribute the global large-scale optimization problem into smaller local subproblems which can be solved in parallel in a decentralized fashion. Thus, reducing the computational burden of the overall approach while obtaining a negligible performance loss with respect to the centralized approach. Moreover, the population-dynamics assistance allows us to satisfy the constraint that couples the multiple local subproblems.

Future research should focus on applying this idea to larger solar plants, such as Solana[3] (808 loops), since the advantages of the coalitional approach with respect to the centralized method become more evident as the plant becomes larger. Additionally, we plan to adapt the proposed coalitional approach to distributed-parameter models of the ACUREX field, which provide a higher level of detail of the field but imply higher complexity in terms of computational load. Other research directions might include the extension of the proposed method to consider the maximization of thermal power by regulating the system's state towards different outlet temperature references.

[3] https://solarpaces.nrel.gov/project/solana-generating-station

CRediT authorship contribution statement

Ana Sánchez-Amores: Methodology, Software, Validation, Formal analysis, Investigation, Data curation, Writing – original draft, Writing – review & editing, Visualization. **Juan Martinez-Piazuelo:** Methodology, Software, Validation, Formal analysis, Investigation, Data curation, Writing – original draft, Writing – review & editing, Visualization, Funding acquisition. **José M. Maestre:** Conceptualization, Methodology, Formal analysis, Writing – review & editing, Supervision, Funding acquisition. **Carlos Ocampo-Martinez:** Conceptualization, Methodology, Formal analysis, Writing – review & editing, Supervision, Funding acquisition. **Eduardo F. Camacho:** Conceptualization, Methodology, Formal analysis, Validation, Supervision, Project administration, Funding acquisition. **Nicanor Quijano:** Conceptualization, Methodology, Formal analysis, Writing – review & editing, Supervision.

Declaration of competing interest

The authors declare that they have no known competing financial interests or personal relationships that could have appeared to influence the work reported in this paper.

Data availability

Data will be made available on request.

References

[1] United nations sustainable development. United Nations, URL https://www.un.org/sustainabledevelopment/. [Accessed 29 July 2022].

[2] Şen Z. Solar energy in progress and future research trends. Prog Energy Combust Sci 2004;30(4):367–416.

[3] Islam MT, Huda N, Abdullah A, Saidur R. A comprehensive review of state-of-the-art concentrating solar power (CSP) technologies: Current status and research trends. Renew Sustain Energy Rev 2018;91:987–1018.

[4] Zhang H, Baeyens J, Degrève J, Cacères G. Concentrated solar power plants: Review and design methodology. Renew Sustain Energy Rev 2013;22:466–81.

[5] Gálvez-Carrillo M, De Keyser R, Ionescu C. Nonlinear predictive control with dead-time compensator: Application to a solar power plant. Sol Energy 2009;83(5):743–52.

[6] Zhu G, Wendelin T, Wagner MJ, Kutscher C. History, current state, and future of linear Fresnel concentrating solar collectors. Sol Energy 2014;103:639–52.

[7] Zhou X, Xu Y. Solar updraft tower power generation. Sol Energy 2016;128:95–125, Special issue: Progress in Solar Energy.

[8] Stefanovic VP, Pavlovic SR, Bellos E, Tzivanidis C. A detailed parametric analysis of a solar dish collector. Sustain Energy Technol Assess 2018;25:99–110.

[9] Alsharkawi A, Rossiter J. Dual mode MPC for a concentrated solar thermal power plant. In: Proceedings of the 11^{Th} IFAC symposium on dynamics and control of process systems, including biosystems. Vol. 49. No. 7. 2016, p. 260–5.

[10] Vasallo MJ, Bravo JM. A MPC approach for optimal generation scheduling in CSP plants. Appl Energy 2016;165(C):357–70.

[11] Ruiz-Moreno S, Frejo JRD, Camacho EF. Model predictive control based on deep learning for solar parabolic-trough plants. Renew Energy 2021;180:193–202.

[12] Escaño JM, Gallego AJ, Sánchez AJ, Yebra LJ, Camacho EF. Nonlinear fuzzy model predictive control of the TCP-100 parabolic trough plant. In: Joint proceedings of the 19th world congress of the international fuzzy systems association (IFSA), the 12th conference of the European society for fuzzy logic and technology (EUSFLAT), and the 11th international summer school on aggregation operators. Atlantis Press; 2021, p. 235–41.

[13] Maestre J, Ridao M, Kozma A, Savorgnan C, Diehl M, Doan M, et al. A comparison of distributed MPC schemes on a hydro-power plant benchmark. Optim Control Appl Methods 2015;36(3):306–32.

[14] Masero E, Frejo JRD, Maestre JM, Camacho EF. A light clustering model predictive control approach to maximize thermal power in solar parabolic-trough plants. Sol Energy 2020;214:531–41.

[15] Masero E, Maestre JM, Camacho EF. Market-based clustering of model predictive controllers for maximizing collected energy by parabolic-trough solar collector fields. Appl Energy 2022;306:117936.

[16] Hofbauer J, Sigmund K. Evolutionary games and population dynamics. Cambridge University Press; 1998.

[17] Sandholm WH. Population games and evolutionary dynamics. MIT Press; 2010.

[18] Quijano N, Ocampo-Martinez C, Barreiro-Gomez J, Obando G, Pantoja A, Mojica-Nava E. The role of population games and evolutionary dynamics in distributed control systems: The advantages of evolutionary game theory. IEEE Control Syst Mag 2017;37(1):70–97.

[19] Tembine H, Altman E, El-Azouzi R, Hayel Y. Evolutionary games in wireless networks. IEEE Trans Syst Man Cybern B 2010;40(3):634–46.

[20] Pashaie A, Pavel L, Damaren CJ. A population game approach for dynamic resource allocation problems. Internat J Control 2017;90(9):1957–72.

[21] Srikantha P, Kundur D. Resilient distributed real-time demand response via population games. IEEE Trans Smart Grid 2017;8(6):2532–43.

[22] Martinez-Piazuelo J, Quijano N, Ocampo-Martinez C. Decentralized charging coordination of electric vehicles under feeder capacity constraints. IEEE Trans Control Netw Syst 2022;9(4):1600–10.

[23] Arcak M, Martins NC. Dissipativity tools for convergence to Nash equilibria in population games. IEEE Trans Control Netw Syst 2021;8(1):39–50.

[24] Pipino HA, Morato MM, Bernardi E, Adam EJ, Normey-Rico JE. Nonlinear temperature regulation of solar collectors with a fast adaptive polytopic LPV MPC formulation. Sol Energy 2020;209:214–25.

[25] Camacho EF, Berenguel M, Rubio FR. Advanced control of solar plants. London: Springer London; 1997.

[26] Camacho EF, Berenguel M, Rubio FR, Martínez D. Control of solar energy systems. London: Springer London; 2012.

[27] Law EW, Prasad AA, Kay M, Taylor RA. Direct normal irradiance forecasting and its application to concentrated solar thermal output forecasting – A review. Sol Energy 2014;108:287–307.

[28] Garcia Martin J, Maestre J. Spatial irradiance estimation in a thermosolar power plant by a mobile robot sensor network. Sol Energy 2021;220:735–44.

[29] Ocampo-Martinez C, Bovo S, Puig V. Partitioning approach oriented to the decentralised predictive control of large-scale systems. J Process Control 2011;21(5):775–86, Special Issue on Hierarchical and Distributed Model Predictive Control.

[30] Martinez-Piazuelo J, Quijano N, Ocampo-Martinez C. Nash equilibrium seeking in full-potential population games under capacity and migration constraints. Automatica 2022;141:110285.

[31] Barreiro-Gomez J, Dörfler F, Tembine H. Distributed robust population games with applications to optimal frequency control in power systems. In: Proceedings of the 2018 annual American control conference. 2018, p. 5762–7.

[32] Barreiro-Gomez J, Tembine H. Constrained evolutionary games by using a mixture of imitation dynamics. Automatica 2018;97:254–62.

[33] Qu G, Li N. On the exponential stability of primal-dual gradient dynamics. IEEE Control Syst Lett 2019;3(1):43–8.

[34] Frejo JRD, Camacho EF. Centralized and distributed model predictive control for the maximization of the thermal power of solar parabolic-trough plants. Sol Energy 2020;204:190–9.